Coordination of Ferrocenyl Ligands Bearing bipy Subunits: Electrochemical, Structural and Spectroscopic Studies

Ana Ion,[a] Mihai Buda,[a] Jean-Claude Moutet,*[b] Eric Saint-Aman,[b] Guy Royal,[b] Isabelle Gautier-Luneau,[c] Michel Bonin,[d] and Raymond Ziessel[e]

Keywords: N ligands / Sandwich complexes / Iron / Receptors / Cyclic voltammetry

The coordinative properties of mono(bipy) and bis(bipy) (bipy refers to 6- or 6,6′-substituted 2,2′-bipyridine) carbonyloxy- and carboxamido-bridged derivatives of ferrocene $\mathbf{L^{1-5}}$ towards a number of metal cations (Cu^{I}, Cu^{II}, Ni^{II}, Fe^{II}, Co^{II}, Hg^{II}, Pb^{II}, Ag^{I}) have been investigated by the interplay of voltammetry, mass spectrometry and X-ray diffraction studies. Particular attention was paid to the electrochemical recognition properties of these redox-active ligands, as monitored by modulation of the ferrocene/ferricinium redox couple upon complexation. It was found that the bis(bipy)-bridged ligands exhibit a *sandwich effect* that gives rise to a well-behaved voltammetric wave for the ferrocene fragment as an elegant signature of complexation. The ferrocenyl ester-bridged bis(bipy) ligand $\mathbf{L^2}$ forms a 2:2 complex in the solid state with Cu^{I}, while the crystal structure of the Cu^{II} complex reveals 1:1 stoichiometry. Upon dissolution, the 2:2 species dissociate rapidly into the $[Cu\mathbf{L^2}]^{+}$ complex. Finally, electrochemical and FAB-MS data have been used to conclude that these ferrocenyl ligands bind to iron(II) to generate unusual $[Fe(bipy)_2]^{2+}$-type complexes.

Introduction

Molecular structures comprising two or more coordinated cations are of considerable interest as reversible electron reservoirs able to effect the successive release of electrons. Such polynuclear metal complexes are also useful models for studying the effect of electronic coupling between metal centres in different oxidation states and for the coupling of a remote redox-active metal centre to a putative catalytic site. In earlier work, it was demonstrated that polypyridine ligands functionalized with ferrocene[1−4] could be used for the electrochemical recognition of certain metal cations in both homogeneous solution[1,2] and polymeric films,[3] and that the resultant dinuclear complexes displayed significant levels of electronic coupling between the metal sites. In extending this work, we now report on the complexation of selected metal cations (Cu^{I}, Cu^{II}, Ni^{II}, Fe^{II}, Co^{II}, Hg^{II}, Pb^{II}, Ag^{I}) with 1-bipy (bipy = 2,2′-bipyridine) and carbonyloxy- or carboxamide-bridged 1,1′-bis(bipy) derivatives of ferrocene (ligands $\mathbf{L^{1-5}}$, Scheme 1). Special attention has been given to studying the effect of cation binding on the electrochemical properties of the ferrocene units.

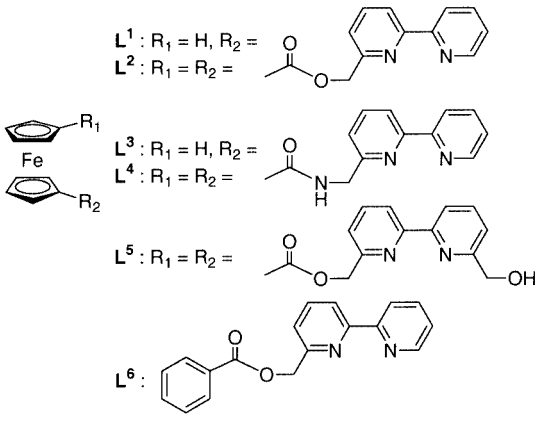

Scheme 1. Structures of ligands $\mathbf{L^{1-6}}$

In a preliminary study,[1] it was reported that the ester-bridged mono(bipy) and bis(bipy) derivatives of ferrocene ($\mathbf{L^1}$ and $\mathbf{L^2}$) are able to complex Cu^{I} and Cu^{II} by ensuring a bis(bipyridyl) environment around the bound cation. The crystal structure of the complex formed between $\mathbf{L^2}$ and Cu^{I} revealed the formation of a 2:2 (2 Cu^{I} + 2 $\mathbf{L^2}$) complex

[a] Department of Applied Physical Chemistry and Electrochemistry, Politehnica University, Bucharest, Romania
[b] Laboratoire d'Electrochimie Organique et de Photochimie Rédox, UMR CNRS 5630, Université Joseph Fourier Grenoble 1, BP 53, 38041 Grenoble Cédex 9, France
Fax: (internat.) + 33-4/76514267
E-mail: Jean-Claude.Moutet@ujf-grenoble.fr
[c] Laboratoire de Chimie Biomimétique, LEDSS, UMR CNRS 5616, Université Joseph Fourier Grenoble 1, BP 53, 38041 Grenoble Cédex 9, France
[d] University of Lausanne, Institute of Crystallography, BSP, 1015 Lausanne, Switzerland
[e] Laboratoire de Chimie, d'Electronique et de Photonique Moléculaires, Ecole de Chimie, Matériaux et Polymères, Université Louis Pasteur, 25 rue Becquerel, 67087 Strasbourg Cédex 02, France

having a *pseudo*-tetrahedral geometry around each cation. The molecular structure was best described as a double-stranded metallo-helicate, with each ligand wrapping around the two copper cations. X-ray structural determination of the $\mathbf{L^2}$ + Cu^{II} complex remains elusive at this time. However, the formation of a mononuclear Cu^{II} complex was evident from EPR experiments. It was further shown that redox ligands $\mathbf{L^1}$ and $\mathbf{L^2}$ recognize copper cations by way of a large shift in the ferrocene/ferricinium (Fc/Fc^+) redox couple. Recently,[2] the formation of bis(bipy)Fe^{II} species upon coordination of Fe^{II} with the carboxamide-bridged mono- and bis(bipy) derivatives $\mathbf{L^{3,4}}$ was deduced from voltammetry, ^1H NMR spectroscopy, FT-IR spectroscopy and mass spectrometry studies. Furthermore, X-ray structural determination of the 1:1 $\mathbf{L^4}$ + Fe^{II} complex showed that the Fe^{II} coordination environment is provided by four nitrogen atoms belonging to the bipy subunits and by two oxygen atoms of the carbonyl groups lying in a "*cis*" environment and describing a distorted octahedral arrangement.

In this paper, we describe the coordination chemistry of copper cations with these ligands, paying particular attention to the complexation process between $\mathbf{L^2}$ and Cu^I. Furthermore, the possibility of obtaining a complex involving an Fe^{II} cation in a bis(bipy) environment from the ester-bridged derivatives $\mathbf{L^{1,2}}$ is also examined, as well as the electrochemical recognition properties of ligands $\mathbf{L^{1-5}}$ towards Ni^{II}, Co^{II}, Hg^{II}, Pb^{II} and Ag^I metal cations.

Results and Discussion

The electrochemical behaviour of the free ligands $\mathbf{L^{1-5}}$ in CH_3CN or CH_2Cl_2 solution is characterized by a one-electron, reversible wave that can be attributed to the ferrocene/ferricinium (Fc/Fc^+) redox couple (Table 1). The main purpose of the current investigation is to examine how complexation of $\mathbf{L^{1-5}}$ by various metal cations (Cu^I, Cu^{II}, Ni^{II}, Fe^{II}, Co^{II}, Hg^{II}, Pb^{II}, Ag^I) affects the electrochemical properties of the ferrocene unit.

Table 1. Electrochemical data for free ligands

[a]	$\mathbf{L^1}$	$\mathbf{L^2}$	$\mathbf{L^3}$	$\mathbf{L^4}$	$\mathbf{L^5}$
CH_3CN	0.33[b]	0.56[b]	0.26[c]	0.53[c]	0.59
CH_2Cl_2	0.45[b]	0.69[b]	[d]	0.51[c]	[d]

[a] $E_{1/2}$ [V] vs. $Ag/AgNO_3$ (0.01 M) + CH_3CN + TBAP (0.01 M), measured by CV at 0.1 V s^{-1}. [b] From ref.[1] [c] From ref.[3] [d] Not determined.

In general, addition of increasing amounts of a given metal cation to a solution of ferrocenyl ligand might be expected to cause one of two effects on the electrochemical activity of the Fc centre. First, cation complexation might induce a gradual positive shift in the Fc/Fc^+ redox potential (one-wave behaviour) due to electrostatic repulsion between the bound cation and the electrogenerated positive charge on the oxidized ferrocenyl subunit. This leads to a decrease of the association constant K_+ with the oxidized ligand and to a destabilisation of the resulting complex.[5] Consequently, $\Delta E_{1/2}$ reflects the balance of interactions between the neutral and charged ligand in its oxidized form with the adventitious metal cation.

Second, we might observe the growth of a new redox wave (two-wave behaviour) at the expense of the original wave for the free ligand. The two-wave behaviour can be linked to a high binding constant K with the neutral ligand in association with a large K/K_+ ratio.[6] It may also, in part, be due to a structural effect i.e. complexation of the binding centre can lead to noncoplanarity of the Cp rings in the complex which is known to result in a marked positive potential shift in complexed[5,7] or strained[8] ferrocenophanes. It should be emphasized that a two-wave feature allows the amperometric recognition and titration of the guest cation, while a one-wave behaviour allows a potentiometric titration.

In general, mono(bipy) ligands $\mathbf{L^1}$ and $\mathbf{L^3}$ form 1:2 (metal/ligand) complexes and give rise to weak complexation and one-wave behaviour, while bis(bipy) ligands $\mathbf{L^2}$ and $\mathbf{L^4}$ form 1:1 complexes and give rise to two-wave behaviour. The bis(bipy) ligand $\mathbf{L^5}$ forms 1:1 complexes, but shows reduced bonding and one-wave behaviour.

In addition to the change in the electroactivity of the Fc centre, the rise of new redox peak systems due to the formation of an electroactive metal complex can be observed in the CV profile. When the emergent complex is fairly stable, all the electrochemical perturbations reach full development at a metal cation/ligand mol ratio corresponding to the stoichiometry of the resultant complex.

Complexation of $\mathbf{L^{1-5}}$ with Cu^I and Cu^{II} Cations

The electrochemical data for complexes formed between $\mathbf{L^{1-5}}$ and Cu^I are summarized in Table 2. The relatively high Cu^I/Cu^{II} redox potential found for these complexes are in good agreement with those reported previously for various copper polypyridyl compounds.[9] In comparative experiments, we found that the reversible $Cu^{I/II}$ oxidation for the $[Cu(bipy)_2]^+$ complex occurs at $E_{1/2} = -0.19$ V, and at 0.26 V for the $[Cu(\mathbf{L^6})_2]^+$ complex where $\mathbf{L^6}$ is a bipy ligand simply mono-substituted with an electron-withdrawing carbonyloxy group.

Table 2. Electrochemical data for $\mathbf{L^1}$, $\mathbf{L^2}$, $\mathbf{L^3}$, $\mathbf{L^4}$, $\mathbf{L^5}$ + Cu^I

[a]	2 $\mathbf{L^1}$ + Cu^I [b]		$\mathbf{L^2}$ + Cu^I [b]		2 $\mathbf{L^3}$ + Cu^I	
	Fc/Fc^+	Cu^I/Cu^{II}	Fc/Fc^+	Cu^I/Cu^{II}	Fc/Fc^+	Cu^I/Cu^{II}
CH_3CN	0.38	0.19	0.71	0.10	0.37	−0.04
CH_2Cl_2	ads.	0.33	0.84	0.23	[c]	[c]
	$\mathbf{L^4}$ + Cu^I		$\mathbf{L^5}$ + Cu^I			
	Fc/Fc^+	Cu^I/Cu^{II}	Fc/Fc^+	Cu^I/Cu^{II}		
CH_3CN	0.60	−0.20	0.64	0.08		
CH_2Cl_2	0.67	−0.15	[c]	[c]		

[a] $E_{1/2}$ [V] vs. $Ag/AgNO_3$ (0.01 M) (see Table 1). [b] From ref.[1] [c] Not determined.

Complexation of $\mathbf{L^1}$ and $\mathbf{L^5}$ with Cu^I in CH_3CN solution results in a one-wave behaviour for the electrochemical response of the Fc centre, along with the rise of a redox peak system attributable to the complexed Cu^I/Cu^{II} redox couple (Table 2). The positive potential shift in the Fc/Fc^+ wave is equal to 50 mV for both ligands. Similar features in the CV behaviour of $\mathbf{L^1}$ and $\mathbf{L^5}$ are evident upon addition of Cu^I or Cu^{II}. Maximal potential shift of the Fc/Fc^+ wave and maximal intensity of the complexed Cu^I/Cu^{II} peak system are obtained at a $Cu^I/\mathbf{L^1}$ and $Cu^I/\mathbf{L^5}$ molar ratio equal to 0.5 and 1, respectively. This result is in keeping with the formation of $[Cu(\mathbf{L^1})_2]^+$ and $[Cu\mathbf{L^5}]^+$ complexes that provide for a bis(bipyridyl) environment around the bound cation. The 1:2 stoichiometry for isolated $[Cu(\mathbf{L^1})_2]^+$ was previously established.[1]

The complexation of $\mathbf{L^{2-4}}$ with Cu^I cations causes the emergence of a new redox peak system (two-wave behaviour) corresponding to the complexed Fc/Fc^+ redox couple

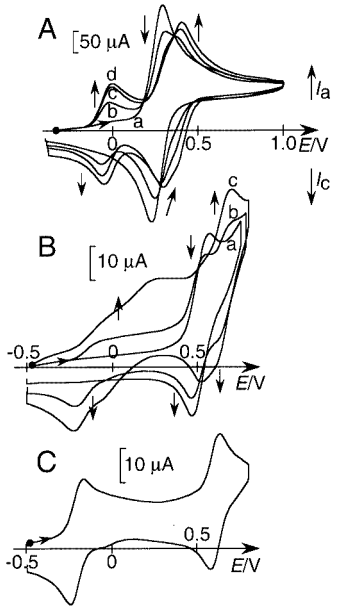

Figure 1. Cyclic voltammograms at a Pt disk (5 mm diameter) of (A) $\mathbf{L^3}$ (2.9 mM) in CH_3CN + TBAP 0.1 M: (a) free $\mathbf{L^3}$; (b) $\mathbf{L^3}$ + 0.2 Cu^+; (c) $\mathbf{L^3}$ + 0.4 Cu^+; (d) $\mathbf{L^3}$ + 0.5 Cu^+; (B) $\mathbf{L^4}$ (1.2 mM) in CH_2Cl_2 + TBAP 0.1 M: (a) free $\mathbf{L^4}$; (b) $\mathbf{L^4}$ + 0.5 Cu^+; (c) $\mathbf{L^4}$ + 1.0 Cu^+; (C) $[Cu\mathbf{L^4}](ClO_4)$ (0.5 mM) in CH_3CN + TBAP 0.1 M; scan rate 0.1 V s^{-1}

(see Figure 1, for example). Due to poor solubility of $\mathbf{L^4}$ in CH_3CN, complexation of this ligand with Cu^I was studied in CH_2Cl_2 (see B in Figure 1). The electrochemical data in CH_3CN solution were obtained, starting with the isolated $\mathbf{L^4}$ + Cu^I complex (see C in Figure 1).

A CV titration shows that the apparent stoichiometry of the complexes formed between $\mathbf{L^2}$, $\mathbf{L^3}$, or $\mathbf{L^4}$ and Cu^I or Cu^{II} is equal to 1:1, 1:2 and 1:1 (metal cation/ligand), respectively. The stoichiometry has been confirmed by MS data. The FAB-MS spectra of the isolated complexes exhibit peaks at m/z = 673 ($[Cu\mathbf{L^2}]^+$); 957 and 857 $\{[Cu(\mathbf{L^3})_2](ClO_4)^+$ and $[Cu(\mathbf{L^3})_2]^+$, respectively$\}$; 771 and 671 $\{[Cu\mathbf{L^4}](ClO_4)^+$ and $[Cu\mathbf{L^4}]^+$, respectively$\}$.

Complexation of Cu^I or Cu^{II} by $\mathbf{L^2}$ has been further studied. We reported previously that the crystal structure of the complex formed between $\mathbf{L^2}$ and Cu^I reveals the formation of a 2:2 (2 Cu^I + 2 $\mathbf{L^2}$) metallo-helicate complex, while the formation of a mononuclear Cu^{II} complex is evident from EPR experiments.[1] The latter result has been confirmed in this study where the X-ray structure of the isolated $[Cu\mathbf{L^2}](ClO_4)_2$ complex revealed the formation of a 1:1 complex (vide infra). The question of the conversion in solution between $[Cu_2(\mathbf{L^2})_2]^{2+}$ and $[Cu\mathbf{L^2}]^+$ thus remains to be addressed. In particular, identical electrochemical features, i.e. superimposable CV curves and same potentials for both complexed Cu^I/Cu^{II} and Fc/Fc^+ redox couples, were obtained following the addition of Cu^{II} instead of Cu^I. In addition, no change in the $E_{1/2}$ value and in the reversibility of the Cu^I/Cu^{II} and Fc/Fc^+ redox couples could be observed in the 5×10^{-2} M (saturated electrolytic solution, prepared from the isolated complex) to 10^{-5} M concentration range, demonstrating that no change occurs in the stoichiometry of the dissolved complex.[1]

Formation of 1:1 and 1:2 complexes from the dimer has been observed by high-resolution ES mass spectrometry upon dissolution of an authentic sample of $[Cu_2(\mathbf{L^2})_2](BF_4)_2$. ES mass spectra were recorded in the 5×10^{-5} to 5×10^{-3} M concentration range. Peaks at m/z (%) = 673.1 (100) and 1283.5 are observed from the ES mass spectra (Figure 2). The isotopic peaks are separated by 1.0 m/z unit, revealing a charge state of +1 for the corresponding ions. Therefore, the peaks at 673.3 and 1283.5 correspond to the $[Cu\mathbf{L^2}]^+$ and $[Cu(\mathbf{L^2})_2]^+$ species, respectively. In addition, the intensity of the peak at 1283.5 appears very weak and decreases with concentration from 1.1% at 5×10^{-3} M down to 0.5% at 5×10^{-5} M, while no peaks characteristic of the $[Cu_2(\mathbf{L^2})_2]^{2+}$ entity or additional peaks corresponding to other species could be detected in the ES-MS spectra. Interestingly, the formation of the 1:1 and 1:2 complexes from the genuine $[Cu_2(\mathbf{L^2})_2](BF_4)_2$ complex should be accompanied with the release of free Cu^I cations. Indeed, a weak peak at 186.7 (not shown in Figure 2) corresponding to $[Cu(CH_3CN)_3]^+$ is simultaneously observed during the ES-MS analyses.

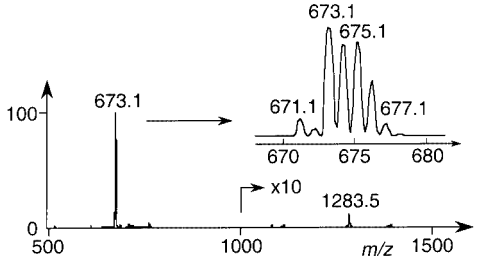

Figure 2. ES-MS spectrum of an acetonitrile solution of authentic $[Cu_2(\mathbf{L^2})_2](BF_4)_2$ (monocrystals) 5×10^{-3} M; Vc = 20 V; insert: isotopic pattern obtained for the peak at m/z = 673.1

On the basis of the electrochemical and electrospray mass spectrometry results, it can be clearly concluded that the 2:2 complex $[Cu_2(\mathbf{L^2})_2]^{2+}$ does not survive upon dissolution and dissociates rapidly to mainly form a 1:1 complex, along

with a minor 1:2 complex. The latter is not detected electrochemically and fully reversible CV behaviour is observed with Cu^{II} or Cu^{I} + $\mathbf{L^2}$ accounting for the reversible electroactivity of the 1:1 complex.

Comparing the electrochemical results obtained from $\mathbf{L^1}$−$\mathbf{L^5}$, we can highlight the benefit of a bis(bipyridyl)-bridged ferrocene ligand with respect to the electrochemical recognition of the metal cation. Complexation of $\mathbf{L^1}$ with copper leads to a one-wave feature for the Fc centre, while $\mathbf{L^2}$ allows amperometric titration of the copper through a two-wave behaviour for its Fc centre. However, complexation of the mono-substituted ligand $\mathbf{L^3}$ is responsible for an unexpected two-wave feature, although the wave corresponding to the complexed ferrocene centre partially overlaps that of the free ligand (see A in Figure 1). In contrast, the bis(bipyridyl)-bridged ligand $\mathbf{L^5}$ shows one-wave behaviour upon complexation of copper. As expected, the recognition properties of a given ligand are linked to its complexation ability. The presence of two additional electron-withdrawing groups in $\mathbf{L^5}$ and steric constraints imposed by the additional 6′-substitution in $\mathbf{L^5}$, as compared to $\mathbf{L^2}$, are responsible for weaker complexation and thus, for a decrease in its electrochemical recognition ability.

X-ray Molecular Structures of the Cu^{II} and Ni^{II} Complexes of Ligand L^2

The crystal structures of both complexes $\{Cu^{II}\mathbf{L^2}\}$ and $\{Ni^{II}\mathbf{L^2}\}$ reveal a 1:1 stoichiometry. The two compounds crystallize in the *C*2/*c* space group revealing 1.5 crystallographically independent dicationic molecular entities (Table 3). One entity is on the general position, and the second is lying on a twofold axis passing through the Fe and M^{II} (Cu2 or Ni2) atoms. The ORTEP view of the dicationic entities $[Cu\mathbf{L^2}]^{2+}$ is shown in Figure 3. The same atom labels are used in both complexes. Selected distances and bond angles of the two complexes are given in Table 4.

{$Cu^{II}L^2$}

The Cu^{II} environment is provided by four nitrogen atoms of the bipy subunits and two oxygen atoms of the carbonyl functions leading to a distorted octahedral coordination geometry. The square planes around Cu1 and Cu2 are defined by atoms O2, N1, N2, N3 and O6A, N5, N6, N5A, respectively (the mean-square deviations are 0.166 Å and 0.086 Å, respectively). The O4, N4 atoms and O6, N6 atoms occupy the axial positions, with the N4−Cu1−O4 and N6−Cu2−O6 angles equal to 168.7(1)° and 165.2(2)°, respectively. The Cu−N distances vary between 1.991(4) Å and 2.091(4) Å, and related Cu−O distances are significantly longer with Cu1−O2 = 2.226(4) Å and Cu1−O4 = 2.483(4) Å. The oxygen atoms adopt a *cis* position. The bipy units are slightly twisted (torsion angles between the cycles are equal to N1C5C6N2 = 4.7°; N3C25C26N4 = 12.1°; N5C45C46N6 = 10.1°). The cyclopentadienyl rings are almost parallel [the tilt angles are equal to 1.0(3)° for Fe1 and 0.35(20)° for Fe2] and the distances from the iron atom to the centroids of these planes are very similar [Fe1: 1.644(3) Å; Fe2: 1.639(3) Å]. An important observation is that the intermetallic distances [Fe1···Cu1 5.309(1) Å, Fe2···Cu2 5.153(2) Å] are far too long for any direct metal−metal interaction to be invoked.

{$Ni^{II}L^2$}

The Ni^{II} complex is isostructural with the Cu^{II} complex, the cation being surrounded by four nitrogen atoms provided by the bipyridine subunits and two oxygen atoms of

Table 3. Crystal data and structure refinement for $[Cu\mathbf{L^2}](ClO_4)_2$ and $[Ni\mathbf{L^2}](ClO_4)_2$

	$[Cu\mathbf{L^2}](ClO_4)_2$	$[Ni\mathbf{L^2}](ClO_4)_2$
Empirical formula	$C_{58}H_{51.5}Cl_3Cu_{1.5}Fe_{1.5}N_{8.5}O_{18.5}$	$C_{58}H_{53.5}Cl_3Ni_{1.5}Fe_{1.5}N_{7.5}O_{19}$
Formula mass	1449.01	1437.77
Crystal system	monoclinic	monoclinic
Space group	*C*2/*c*	*C*2/*c*
a [Å]	16.482(3)	16.161(3)
b [Å]	22.383(5)	22.441(5)
c [Å]	33.389(7)	34.264(7)
β [°]	98.47(3)	96.27(3)
V [Å^3]/Z	12348(4)/8	12352(8)/8
D_X [g cm^{-3}]	1.559	1.546
μ [cm^{-1}]	10.69	10.10
Crystal dim. [mm]	0.05 × 0.05 × 0.15	0.05 × 0.07 × 0.15
Shape/colour	needle/brown-dark	needle/green-dark
T [K]	200	170
$2\theta_{max}$ [°]	48	48.5
Number of reflections collected	27068	38058
Restraints/parameters	72/915	65/873
$R(F)$[a]	0.0561 for $I > 2\sigma(I)$	0.0525 for $I > 2\sigma(I)$
$R_w(F^2)$[b]	0.1739	0.1701
Goodness of fit *S*	1.02	0.83
$\Delta\rho_{min}/\Delta\rho_{max}$ [e Å^{-3}]	−0.57/0.96	−0.51/0.83

[a] $R = \Sigma||F_o| - |F_c||/\Sigma|F_o|$. [b] $R_w = [\Sigma w(|F_o| - |F_c|)^2/[\Sigma w F_o^2]^{1/2}$.

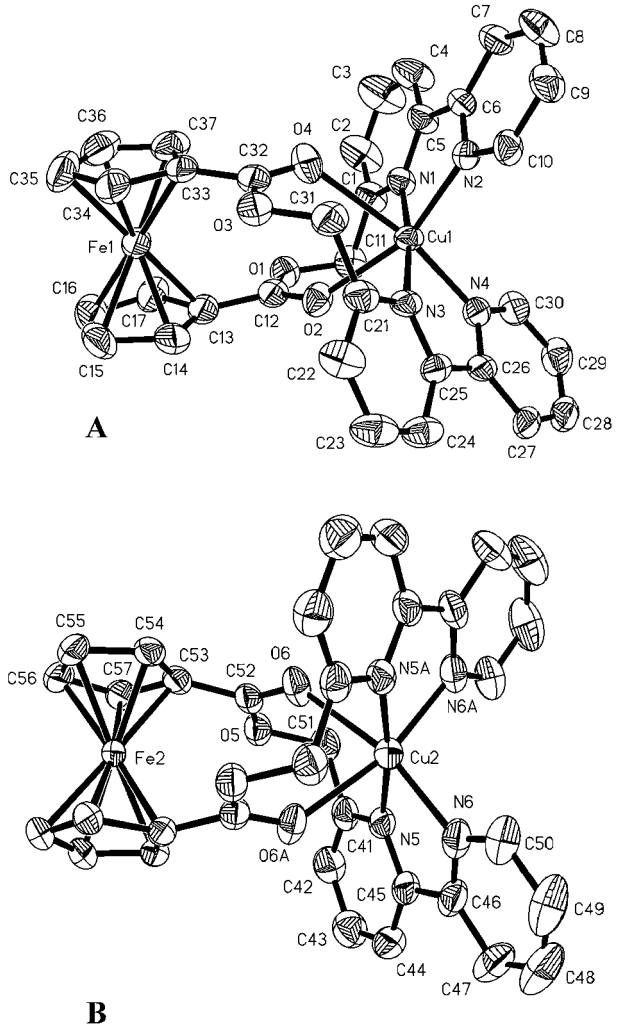

Figure 3. ORTEP plots of the two crystallographically independent units $[Cu\mathbf{L^2}]^{2+}$: (A) entity on general position; (B) entity on a 2-fold axis; hydrogen atoms are omitted for clarity; ellipsoids are drawn at a 30% probability level

Table 4. Selected bond lengths [Å] and bond angles [°] for $[Cu\mathbf{L^2}](ClO_4)_2$ and $[Ni\mathbf{L^2}](ClO_4)_2$ (symmetry equivalent position A = 1 − *x*, *y*, 0.5 − *z*)

$[Cu\mathbf{L^2}](ClO_4)_2$		$[Ni\mathbf{L^2}](ClO_4)_2$	
Cu(1)−Fe(1)	5.307(1)	Ni(1)−Fe(1)	5.072(1)
Cu(2)−Fe(2)	5.154(2)	Ni(2)−Fe(2)	4.963(1)
Cu(1)−N(1)	1.991(4)	Ni(1)−N(1)	2.074(4)
Cu(1)−N(2)	2.031(4)	Ni(1)−N(2)	2.033(4)
Cu(1)−N(3)	2.007(4)	Ni(1)−N(3)	2.060(3)
Cu(1)−N(4)	2.091(4)	Ni(1)−N(4)	2.019(4)
Cu(1)−O(2)	2.226(4)	Ni(1)−O(2)	2.152(3)
Cu(1)−O(4)	2.483(4)	Ni(1)−O(4)	2.145(3)
Cu(2)−N(5)	2.038(5)	Ni(2)−N(5)	2.093(4)
Cu(2)−N(6)	2.073(5)	Ni(2)N(6)	2.031(4)
Cu(2)−O(6)	2.263(4)	Ni(2)−O(6)	2.108(3)
N(1)−Cu(1)−N(2)	82.0(2)	N(1)−Ni(1)−N(2)	80.4(2)
N(1)−Cu(1)−N(3)	174.0(2)	N(1)−Ni(1)−N(3)	177.5(1)
N(2)−Cu(1)−N(3)	101.9(2)	N(2)−Ni(1)−N(3)	98.9(2)
N(1)−Cu(1)−N(4)	102.2(2)	N(1)−Ni(1)−N(4)	102.2(1)
N(2)−Cu(1)−N(4)	108.3(2)	N(2)−Ni(1)−N(4)	98.7(1)
N(3)−Cu(1)−N(4)	81.1(2)	N(3)−Ni(1)−N(4)	80.3(1)
N(1)−Cu(1)−O(2)	94.6(2)	N(1)−Ni(1)−O(2)	95.5(1)
N(2)−Cu(1)−O(2)	158.2(1)	N(2)−Ni(1)−O(2)	173.1(1)
N(3)−Cu(1)−O(2)	80.1(1)	N(3)−Ni(1)−O(2)	84.9(1)
N(4)−Cu(1)−O(2)	93.5(1)	N(4)−Ni(1)−O(2)	87.6(1)
N(1)−Cu(1)−O(4)	79.3(2)	N(1)−Ni(1)−O(4)	82.3(1)
N(3)−Cu(1)−O(4)	96.5(2)	N(3)−Ni(1)−O(4)	95.3(1)
N(2)−Cu(1)−O(4)	83.1(1)	N(2)−Ni(1)−O(4)	93.3(1)
N(4)−Cu(1)−O(4)	168.7(1)	N(4)−Ni(1)−O(4)	167.7(1)
O(2)−Cu(1)−O(4)	75.2(1)	O(2)−Ni(1)−O(4)	80.6(1)
N(5)−Cu(2)−N(6A)	104.2(2)	N(5)−Ni(2)−N(6A)	102.3(2)
N(5)−Cu(2)−N(6)	80.4(2)	N(5)−Ni(2)−N(6)	79.6(2)
N(5)−Cu(2)−N(5A)	172.3(2)	N(5)−Ni(2)−N(5A)	177.1(2)
N(5)−Cu(2)−O(6)	94.7(2)	N(5)−Ni(2)−O(6)	94.7(1)
N(5)−Cu(2)−O(6A)	79.3(2)	N(5)−Ni(2)−O(6A)	83.1(1)
N(6)−Cu(2)−O(6)	165.2(2)	N(6)−Ni(2)−O(6)	170.5(1)
N(6)−Cu(2)−N(5A)	104.2(2)	N(6)−Ni(2)−N(5A)	102.3(2)
N(6)−Cu(2)−N(6A)	107.8(3)	N(6)−Ni(2)−N(6A)	99.7(2)
N(6)−Cu(2)−O(6A)	87.0(2)	N(6)−Ni(2)−O(6A)	88.8(1)
O(6)−Cu(2)−O(6A)	78.4(2)	O(6)−Ni(2)−O(6A)	83.0(2)

the linkers describing a slightly distorted octahedral coordination sphere.

In both structures, the ester groups are almost coplanar with the Cp rings and coordination of the Cu^{II} or Ni^{II} cations by the carbonyl moieties involves a conjugated frame between the ferrocenyl subunit and the metal centres.

Complexation of $\mathbf{L^{1-5}}$ with Ni^{II} Cations

The electrochemical data for complexation of $\mathbf{L^{1-5}}$ with Ni^{II} in the CH_3CN or CH_2Cl_2 electrolyte are summarized in Table 5. In terms of electrochemical response, the recognition properties of these redox-active receptors towards Ni^{II} are similar to that observed with Cu^{I} and Cu^{II}.

Complexation of Ni^{II} with $\mathbf{L^1}$ and $\mathbf{L^5}$ results in a one-wave feature for the Fc centre (e.g. Figure 4A for $\mathbf{L^1}$ + Ni^{II}). Addition of Ni^{II} to a solution of $\mathbf{L^1}$ or $\mathbf{L^5}$ induces a progressive weak positive shift of up to 60 mV in the potential of the Fc/Fc^+ couple. The maximal value is reached when 0.5 and 1 mol-equiv. of Ni^{II} have been added to $\mathbf{L^1}$ and $\mathbf{L^5}$, respectively. This suggests the formation of $[Ni(\mathbf{L^1})_2]^{2+}$ and $[Ni\mathbf{L^5}]^{2+}$ complexes where a bis(bipy) environment is provided for the cation. In the negative potentials range, the $\mathbf{L^1}$ + Ni^{II} system is characterized by two new reversible waves at $E_{1/2} = -0.98$ and -1.45 V (Figure 4A). Their intensity increases linearly with the amount of Ni^{II}, then remains constant after the addition of more than a 0.5 mol equiv. Above 0.5 mol-equiv., the CV curve displays the electrochemical response of free Ni^{II} salts as an irreversible cathodic peak around −1.5 V with the corresponding anodic peak being located around 0.2 V on the reverse scan. As judged by coulometric titration, the two reduction waves correspond to one-electron transfer leading to $[Ni(\mathbf{L^1})_2]^+$ and $[Ni(\mathbf{L^1})_2]^0$, respectively. Unfortunately, the poor stability of the electroreduced species excluded the assignment from EPR studies of the redox orbitals involved in these reductions. In contrast, addition of Ni^{II} to a solution containing $\mathbf{L^5}$ gives rise to an ill-behaved irreversible cathodic wave around −1.2 V and to electrochemical features typical of free Ni^{II}, whatever the nickel concentration used. This indicates the formation of an unlocked complex $[Ni\mathbf{L^5}]^{2+}$, which liberates Ni^{II} cations.

Table 5. Electrochemical data for $\mathbf{L^1}$, $\mathbf{L^2}$, $\mathbf{L^3}$, $\mathbf{L^4}$, $\mathbf{L^5}$ + Ni^{II}

[a]	$2\mathbf{L^1}$ + Ni^{II} Fc/Fc^+	Ni^{II}/Ni^I	Ni^I/Ni^0	$\mathbf{L^2}$ + Ni^{II} Fc/Fc^+	Ni^{II}/Ni^I	Ni^I/Ni^0	$2\mathbf{L^3}$ + Ni^{II} Fc/Fc^+	Ni^{II}/Ni^I	Ni^I/Ni^0
CH_3CN	0.39	−0.98	−1.48	0.80	−1.16	−1.47	0.40	−1.33	−1.48
CH_2Cl_2	0.51	[b]	[b]	0.83	−1.04	−1.42	[c]	[c]	[c]
	$\mathbf{L^4}$ + Ni^{II} Fc/Fc^+	Ni^{II}/Ni^I	Ni^I/Ni^0	$\mathbf{L^5}$ + Ni^{II} Fc/Fc^+	Ni^{II}/Ni^I	Ni^I/Ni^0			
CH_3CN	0.74	[c]	[c]	0.65	[c]	[c]			
CH_2Cl_2	0.73	−1.43	[c]	[c]	[c]	[c]			

[a] $E_{1/2}$ [V] vs. $Ag/AgNO_3$ (0.01 M) (see Table 2). [b] Strong adsorption phenomena precluded determination of $E_{1/2}$. [c] Not determined.

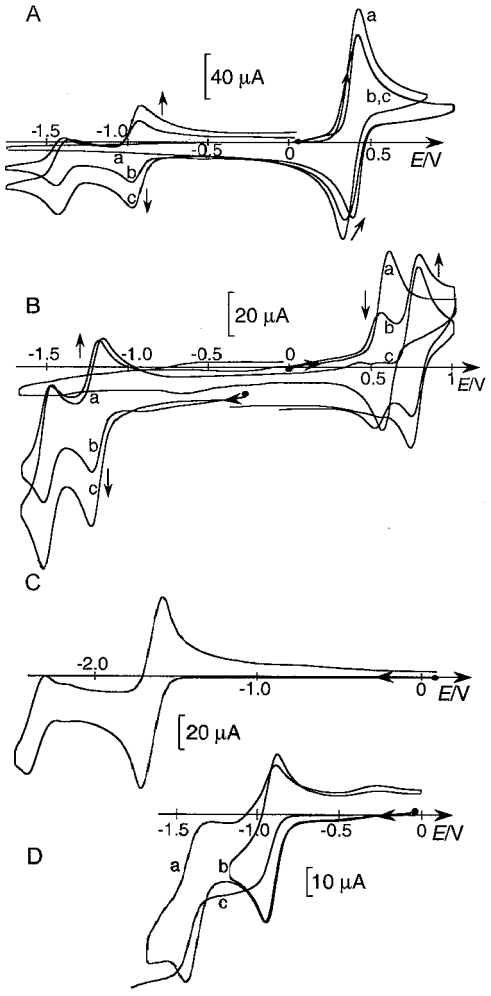

Figure 4. Cyclic voltammograms at $\nu = 0.1$ V s^{-1}, in CH_3CN + TBAP (0.1 M), at a Pt disk (5 mm diameter) of (A) $\mathbf{L^1}$ (2.5 mM): (a) free $\mathbf{L^1}$; (b) $\mathbf{L^1}$ + 0.25 Ni^{2+}; (c) $\mathbf{L^1}$ + 0.5 Ni^{2+}; (B) $\mathbf{L^2}$ (1.2 mM): (a) free $\mathbf{L^2}$; (b) $\mathbf{L^2}$ + 0.5 Ni^{2+}; (c) $\mathbf{L^2}$ + 1.0 Ni^{2+}; (C) $[Ni(bipy)_2](ClO_4)_2$ (0.5 mM); (D) $[Ni(\mathbf{L^6})_2](ClO_4)_2$ (0.5 mM): (a, b) CV curves; (c) RDE voltammetry curve (carbon disk, 3 mm diameter; 600 rev min^{-1}, $\nu = 0.01$ V s^{-1})

The $\mathbf{L^{2-4}}$ + Ni^{II} systems are best characterized by a two-wave behaviour for the Fc/Fc^+ redox couple in the presence of increasing amounts of Ni^{II} (see for example B in Figure 4; $\mathbf{L^2}$ + Ni^{II}). Upon progressive addition of Ni^{II} to $\mathbf{L^2}$, $\mathbf{L^3}$ or $\mathbf{L^4}$ in CH_3CN, a new redox wave corresponding to the complexed Fc/Fc^+ redox couple merges gradually at 0.80, 0.40 and 0.74 V, respectively. At the same time, the redox wave for the free Fc/Fc^+ couple vanishes. The cathodic electrochemical response of the complexes formed between Ni^{II} and $\mathbf{L^2}$ or $\mathbf{L^3}$ is revealed on the CV curves as two successive one-electron waves located at $E_{1/2} = -1.16$ and −1.47 V ($\mathbf{L^2}$; see B in Figure 4), and −1.33 and −1.48 V ($\mathbf{L^3}$). However, it must be noted that the electrochemical recognition properties of $\mathbf{L^3}$ are less marked than those of $\mathbf{L^2}$, for the following reasons: (*i*) the new signal corresponding to the complexed Fc/Fc^+ redox couple partially overlaps that of the free ligand, (*ii*) the two successive cathodic signals are ill-behaved and weakly separated, and (*iii*) a residual signal assigned to the free ligand remains observable in the presence of excess Ni^{II}.

Due to the poor solubility of $\mathbf{L^4}$ in CH_3CN solution, the cathodic features of the Ni^{II} + $\mathbf{L^4}$ system were determined in CH_2Cl_2 solution. In the accessible potential range only the first reduction of the $\mathbf{L^4}$ + Ni^{II} complex could be seen, at $E_{1/2} = -1.43$ V.

All perturbations due to the presence of Ni^{II} in solutions containing ligands $\mathbf{L^2}$, $\mathbf{L^3}$, or $\mathbf{L^4}$ reach their maximum intensity at a mol ratio Ni^{II}/ligand = 1, 0.5, and 1, respectively, suggesting the formation of complexes of the type $[Ni\mathbf{L^2}]^{2+}$, $[Ni(\mathbf{L^3})_2]^{2+}$, and $[Ni\mathbf{L^4}]^{2+}$. The stoichiometry of the $[Ni\mathbf{L^2}]^{2+}$ and $[Ni(\mathbf{L^3})_2]^{2+}$ species was confirmed by UV/Vis titration experiments. The titration curve (absorbance at λ_{max} = 460 nm of a CH_3CN solution of $\mathbf{L^2}$ as a function of increasing amounts of Ni^{II}) exhibits a sharp inflection point at an $Ni^{II}/\mathbf{L^2}$ mol ratio equal to 1 (ε_{max} = 140 M^{-1} cm^{-1}). The titration curve for the $\mathbf{L^3}$ + Ni^{II} complex (λ_{max} = 450 nm; ε_{max} = 500 M^{-1} cm^{-1}) displays an inflection point for $Ni^{II}/\mathbf{L^3} = 0.5$. In addition, FAB-MS spectra of the isolated $[Ni\mathbf{L^2}]^{2+}$ and $[Ni\mathbf{L^4}]^{2+}$ complexes display, exclusively, the *m/z* peaks corresponding to the 1:1 complex: *m/z* = 767 $\{[Ni\mathbf{L^2}](ClO_4)^+\}$ and 765 $\{[Ni\mathbf{L^4}](ClO_4)^+\}$.

The differences in the CV behaviour for these Ni^{II} complexes can be related to the nature of the $\mathbf{L^{1-5}}$ ligand. With $\mathbf{L^1}$ and $\mathbf{L^3}$ two ligands are involved in forming the complexes, while only one ligand is involved in the $\mathbf{L^2}$-, $\mathbf{L^4}$- and $\mathbf{L^5}$-based complexes, pointing to a bis(bipy) environment of the first coordination sphere of the metal centre. The *sand-*

wich effect provided by $\mathbf{L^2}$ or $\mathbf{L^4}$ causes a two-wave behaviour for the Fc/Fc^+ redox centre, while complexation of $\mathbf{L^1}$ or $\mathbf{L^3}$ leads to a simple anodic shift of the Fc oxidation ($\mathbf{L^1}$), or to a poorly resolved new signal ($\mathbf{L^3}$). As already discussed for its complexation with copper cations, the bis(bipy) ligand $\mathbf{L^5}$ shows reduced complexation ability and poor recognition properties.

The electrochemical reduction of nickel complexes proceeds by two successive one-electron transfers. This electrochemical behaviour is markedly different from that found for the complex formed between unsubstituted bipy and Ni^{II}. Under the same experimental conditions, the regular $[Ni(bipy)_2]^{2+}$ complex undergoes two successive, reversible electron transfers at $E_{1/2} = -1.55$ and -2.25 V in CH_3CN (see C in Figure 4). As reported previously,[10] reduction of $[Ni(bipy)_2]^{2+}$ is likely to occur following the $[Ni(bipy)_2]^{2+} \rightarrow [Ni(bipy)_2]^0 \rightarrow [Ni(bipy)_2]^-$ steps, the first step corresponding to a two-electron transfer. However, substitution of the bipy ligand with a simple electron-withdrawing group, as in $\mathbf{L^6}$, causes a dramatic change in this electrochemical mechanism. The CV curve recorded for Ni^{II} + 2 $\mathbf{L^6}$ in CH_3CN exhibits two reversible waves with comparable intensities at $E_{1/2} = -0.94$ and -1.43 V (see D in Figure 4). Further reduction is observed at a lower potential as an irreversible peak ($E_{1/2} = -2.02$ V, determined from RDE experiments). Coulometric titration has demonstrated that the three reductions are one-electron transfers, according to the following sequence: $[Ni(\mathbf{L^6})_2]^{2+} \rightarrow [Ni(\mathbf{L^6})_2]^{+} \rightarrow [Ni(\mathbf{L^6})_2]^0 \rightarrow [Ni(\mathbf{L^6})_2]^-$. Two additive effects could be responsible for such a change in the electrochemical behaviour of these complexes. It is obvious that substitution of the bipyridyl-binding site in $\mathbf{L^{1-6}}$ by electron-withdrawing groups leads to a stabilization of the reduced forms of the nickel complexes. Moreover, change in geometry between the unsubstituted bipy complex (likely to be square-planar) and the $\mathbf{L^{1-6}}$ complexes {likely to be octahedral as in $[Ni(\mathbf{L^2})]^{2+}$} might result in different redox properties.

Complexation of $\mathbf{L^{1-5}}$ with Fe^{II} Cations

Electrochemical data for complexation of $\mathbf{L^{1-5}}$ with Fe^{II} are summarized in Table 6. In a recent study,[2] we have shown that the complexation of $\mathbf{L^{3,4}}$ with Fe^{II} results in a two-wave behaviour for the Fc centre and in the formation of 1:2 $\{[Fe(\mathbf{L^3})_2]^{2+}\}$ and 1:1 $\{[Fe\mathbf{L^4}]^{2+}\}$ complexes. However, with $\mathbf{L^3}$ the intermediate formation at a low $Fe^{II}/\mathbf{L}$ ratio of the $[Fe(\mathbf{L^3})_3]^{2+}$ complex was evidenced from electrochemical experiments and UV/Vis titration.

Replacement of the amide linkage in $\mathbf{L^3}$ with the carbonyloxy linkage in $\mathbf{L^1}$ leads to strong modifications in the complexation pathway. Complexation of $\mathbf{L^1}$ with Fe^{II} in CH_3CN results in a one-wave behaviour of the electrochemical response for the Fc centre, which shifts from 0.33 V in free $\mathbf{L^1}$ to 0.37 V in the presence of excess Fe^{II}. The electrochemical response of the Fe^{II}/Fe^{III} redox couple in the $\mathbf{L^1}$-based complex is seen at $E_{1/2} = 0.95$ V, a value close to that found for $[Fe(\mathbf{L^3})_2]^{2+}$,[2] without any CV evidence for the intermediate formation of an "$Fe(bipy)_3$"-like species. The potentiometric titration curve displays a smooth inflection point around 0.5 mol-equiv. of Fe^{II}, which suggests the formation of an $[Fe(\mathbf{L^1})_2]^{2+}$ complex.

Table 6. Electrochemical data for $\mathbf{L^1}$, $\mathbf{L^2}$, $\mathbf{L^3}$, $\mathbf{L^4}$, $\mathbf{L^5}$ + Fe^{II}

[a]	$2\mathbf{L^1}$ + Fe^{II}		$\mathbf{L^2}$ + Fe^{II}		$2\mathbf{L^3}$ + Fe^{II}	
Fc/Fc^+	Fe^{II}/Fe^{III}		Fc/Fc^+	Fe^{II}/Fe^{III}	Fc/Fc^+	Fe^{II}/Fe^{III}
0.37	0.95		0.78[b]	0.98[b]	0.39[c]	0.97[c]
	$3\mathbf{L^3}$ + Fe^{II}		$\mathbf{L^4}$ + Fe^{II}		$\mathbf{L^5}$ + Fe^{II}	
Fc/Fc^+	Fe^{II}/Fe^{III}		Fc/Fc^+	Fe^{II}/Fe^{III}	Fc/Fc^+	Fe^{II}/Fe^{III}
0.39[c]	0.77[c]		0.64[c] [d]	0.99[c,d]	0.83[b]	0.98[b]

[a] $E_{1/2}$ [V] vs. $Ag/AgNO_3$ (0.01 M) (see Table 2), measured in CH_3CN electrolyte. [b] Irreversible oxidation. [c] From ref.[1] [d] $E_{1/2} = 0.73$ and 0.95 V in CH_2Cl_2.

In contrast, addition of Fe^{II} to a solution of $\mathbf{L^2}$ or $\mathbf{L^5}$ results in the appearance of a new Fc/Fc^+ oxidation wave at $E_{1/2} = 0.78$ and 0.83 V, respectively, at the expense of the free ligand (Figure 5). This wave reaches full development at an Fe^{II}/ligand mol ratio of 1 (Figure 5, curve b), suggesting the formation of 1:1 complexes in which the Fe^{II} centre is bound to two bipyridyl sites provided by the same metallo ligand, as established for bis(bipy)− and bis(phen)−ferrocene derivatives.[2] The stoichiometry of the complex $\mathbf{L^2}$ + Fe^{II} was confirmed from UV/Vis titration. Addition of Fe^{II} in a CH_3CN solution of $\mathbf{L^2}$ results in the appearance of an MLCT band ($\lambda_{max} = 450$ nm) of increasing intensity until 1 mol-equiv. of Fe^{II} has been added ($\varepsilon_{max} = 1.1 \times 10^3$ M^{-1} cm^{-1}). This result was further confirmed by the FAB mass spectrum of the isolated complex which displays peaks at $m/z = 765$ $\{[Fe\mathbf{L^2}](ClO_4)^+\}$ and 666 $\{[Fe\mathbf{L^2}]^{2+} - 1\}$.

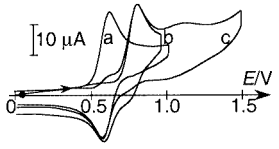

Figure 5. Cyclic voltammograms, in CH_3CN + TBAP (0.1 M), at a Pt disk (5 mm diameter) of 0.4 mM $\mathbf{L^2}$: (a) free $\mathbf{L^2}$; (b) $\mathbf{L^2}$ + 1.0 Fe^{2+} in the 0 to 0.95 V scan range; (c) $\mathbf{L^2}$ + 1.0 Fe^{2+} in the 0 to 1.45 V range; scan rate 0.1 V s^{-1}

However, oxidation of the complexed ligands $\mathbf{L^2}$ and $\mathbf{L^5}$ is irreversible in appearance. On the reverse scan, only the cathodic peak corresponding to the reduction of the ferrocene unit in the free ligand is observed (Figure 5, curve b). Thus, dissociation occurs upon oxidation of the $[Fe\mathbf{L^{2,5}}]^{2+}$ complexes, due to the establishment of repulsive electrostatic forces between the positively charged Fc^+ centre and the dicationic bound metal cation Fe^{II}. Moreover, in addition to the electrochemical signal due to the complexed Fc centre, the anodic response of the bound Fe^{II} cation is evident, on the CV curves, as a broad, ill-behaved irreversible wave at $E_{1/2} = 0.98$ V (determined from RDE experiments) for both complexes (Figure 5, curve c). It should be noted that a small wave corresponding to oxidation of free $\mathbf{L^2}$ re-

mains, even in the presence of a slight excess of Fe^{II}. As for the corresponding copper complexes, the $[FeL^5]^{2+}$ complex is less stable than its $[FeL^2]^{2+}$ analogue. Thus, the oxidation peak for free L^5 is apparent in the CV curves recorded even in the presence of a large excess of Fe^{II} (e.g. 2 mol-equiv.). These results are somewhat different from that found for the $[FeL^4]^{2+}$ complex, which shows reversible CV features. This is in keeping with a weaker binding of the Fe^{II} centre to the carbonyl oxygen atoms of the carbonyloxy group in L^1, compared to the amide donor group in L^3.

In addition, complexes formed from L^1, L^2, or L^5 with Fe^{II} display a broad, irreversible reduction wave at E_p = −1.38 V, −1.35 V, and −2.04 V, respectively. These features confirm that complexation affords species of the type $[Fe(bpy)_2]^{2+}$ rather than $[Fe(bpy)_3]^{2+}$-like complexes. The latter would be characterized by three reversible reduction waves in the negative potential region.

As has already been pointed out for the $[Fe(L^3)_2]^{2+}$ and $[FeL^4]^{2+}$ complexes,[2] ^1H NMR spectra of isolated $[Fe(L^1)_2](ClO_4)_2$ and $[FeL^2](ClO_4)_2$ complexes display resonances in a very large chemical shifts range (from δ = 83 to −10, and from δ = 81 to −9, respectively; see Exp. Sect.), attesting to a high spin configuration for these $\{Fe^{II}(bpy)_2\}$ species. This is confirmed by the rather low molar extinction coefficients of the visible transition in these complexes (600−1600 M^{-1} cm^{-1}; see Exp. Sect.), as compared to that found[11] with low-spin $[Fe(bipy)_2(CH_3CN)_2]^{2+}$ species (ε = 5600 M^{-1} cm^{-1} at 470 nm).

Complexation with Hg^{II}, Pb^{II}, Co^{II} and Ag^I Cations

Electrochemical data obtained in the course of complexation of L^2 with mercury(II), lead(II), cobalt(II) and silver(I) cations are summarized in Table 7. One-wave behaviour was found upon complexation of L^2 with Hg^{II}, with a maximum potential shift of 60 mV for the Fc/Fc^+ redox couple reached at an Hg^{II}/L^2 mol ratio of 1. The Hg^{II} + L^2 complex undergoes a reversible one-electron transfer at $E_{1/2}$ = 0.13 V. This indicates that Hg^I is stabilized upon complexation with L^2, since free Hg^{II} is reduced through a two-electron transfer to form Hg^0 at 0.22 V. Complexation of L^1 with Hg^{II} is also characterized by one-wave behaviour and leads to a lower positive potential shift (30 mV) in the Fc/Fc^+ redox potential, reached at an Hg^{II}/L^1 ratio close to 0.5. These results show the ability of L^1 and L^2 to provide a bipyridyl environment for the Hg^{II} metal cation. The stoichiometry has been further established by MS experiments. The FAB mass spectrum of the isolated L^2 + Hg^{II} complex, prepared as its triflate salt in the presence of an excess of ligand, displays only one peak at *m/z* = 961 $\{[HgL^2](CF_3SO_3)^+\}$ characteristic of a 1:1 complex. Analytical results are also in agreement with the formation of a 1:1 Hg^{II} + L^4 complex with the bis(carboxamide) ligand (see Exp. Sect.).

For Pb^{II}, the one-wave behaviour of the Fc/Fc^+ centre is characterized by a maximum potential shift of 80 mV that is reached at a Pb^{II}/L^2 mol ratio of 1. Reduction of the Pb^{II} + L^2 complex proceeds via several poorly defined steps. In contrast, two-wave behaviour is found upon addition of Co^{II} to L^2. The resultant Fc/Fc^+ redox couple appears at $E_{1/2}$ = 0.79 V, while the weakly reversible Co^{II} centred electron transfer is located at $E_{1/2}$ = 1.1 V. Maximum perturbation is reached at a Co^{II}/L^2 mol ratio of 1. However, the electrochemical signal for free L^2 remains visible on the CV curve even in the presence of excess Co^{II}. Finally, no complexation could be detected upon addition of Ag^I to L^2.

Conclusion

This study confirms the remarkable complexation and electrochemical recognition properties of bipyridyl−ferrocene metallo-synthons for adventitious metal cations. Complexation results in significant positive potential shifts of the ferrocene/ferricinium redox couple following a decrease in the electron density around the ferrocene centre. The bis(substitution) on the ferrocene centre improves the electrical connection between the bound metal cation and the ferrocenyl unit allowing effective electrochemical recognition of the metal cation through a two-wave behaviour for the ferrocene electrochemical response (*sandwich effect*). All the studied ligands afford a bis(bipyridyl) environment for the bound metal cations, which dictates the 1:1 stoichiometry with the bis(substituted) ligands and the 1:2 stoichiometry with the mono(substituted) ligands. In the solid state, Cu^I forms a 2:2 complex with L^2, which does not survive in solution, while Cu^{II} forms a 1:1 complex. The Cu^{II} and Ni^{II} complexes are isostructural with the cations being surrounded by four nitrogen atoms provided by the bipyridine subunits and two oxygen atoms of the linkers. Finally, formation of bis(bipy)-like complexes with Fe^{II} and other metal cations such as Hg^{II}, Pb^{II} and Co^{II} illustrates the wide versatility of the coordination features of these bipy−ferrocenyl ligands.

Experimental Section

Ligands: L^1, L^2, L^3, L^4 and L^5 were synthesized as reported previously.[1,3,4]

Table 7. Electrochemical data for L^2 + Hg^{II}, Pb^{II}, Ag^I and Co^{II}, and L^1 + Hg^{II}

[a] L^2 + Hg^{II}		L^2 + Ag^I	L^2 + Pb^{II}	L^2 + Co^{II}		$2L^1$ + Hg^{II}	
Fc/Fc^+	Hg^{II}/Hg^I	Fc/Fc^+	Fc/Fc^+	Fc/Fc^+	Co^{II}/Co^{III}	Fc/Fc^+	Hg^{II}/Hg^0
0.62	0.13	0.56[b]	0.64	0.79	1.10	0.59	−0.32

[a] $E_{1/2}$ [V] vs. $Ag/AgNO_3$ (0.01 M) (see Table 1), measured in CH_3CN electrolyte. [b] No electrochemical recognition.

L^6: L^6 was prepared according to a similar procedure based on the stoichiometric reaction of 6-(hydroxymethyl)-2,2′-bipyridine[12] with benzoyl chloride. Yield 85%. ^{1}H NMR (300 MHz, CD_3CN, 10 mM, 295 K): δ = 8.66 (1 H, *H*-6′-bipy), 8.41 (1 H, *H*-3-bipy), 8.32 (1 H, *H*-3′-bipy), 8.15 (2 H, *H*-*o*-bz), 7.77−7.87 (2 H, *H*-5-bipy and *H*-4-bipy), 7.44−7.59 (4 H, *H*-*m*-bz, *H*-*p*-bz, *H*-5′-bipy), 7.31 (1 H, *H*-4′-bipy), 5.60 (2 H, CH_2-bipy). FAB$^+$ MS: *m*/*z* = 291 [L^6 + 1]$^+$.

Complexes: All metal complexes were synthesized as their perchlorate or triflate salts, by reaction of stoichiometric amounts of the ligand (40 mg) and the salt of the selected metal cation [1 mol-equiv. in the case of the bis(bipy) derivatives and 0.5 mol-equiv. in the case of mono(bipy)] in a minimum volume of CH_3CN or CH_2Cl_2 at room temperature. The target complexes were precipitated on addition of diethyl oxide and isolated as orange solids by suction filtration (yields 80−90%). X-ray quality crystals were grown by vapour diffusion of diethyl oxide into an acetonitrile solution of the complexes {Cu^{II}L^2} or {Ni^{II}L^2}. [Cu(L^1)$_2$](ClO$_4$), [Cu$_2$(L^2)$_2$](ClO$_4$)$_2$, [Fe(L^3)$_2$](ClO$_4$)$_2$ and [FeL^4](ClO$_4$)$_2$ complexes have been previously described.[1,2] **Warning!** *Perchlorate salts are hazardous because of the possibility of explosion.*

[Cu(L^3)$_2$](ClO$_4$): UV/Vis (MLCT band; CH_3CN): λ_{max} (ε, M^{-1} cm^{-1}) = 442 nm (1718). FAB$^+$ MS: *m*/*z* = 857 [Cu(L^3)$_2$]$^+$. FT-IR: ν(CO) = 1602 cm^{-1}; due to hygroscopic properties, no reproducible elementary analysis could be obtained with this compound.

[CuL^4](ClO$_4$): UV/Vis (MLCT band; CH_3CN) λ_{max}, (ε, M^{-1} cm^{-1}) = 444 nm (3250). FAB$^+$ MS: *m*/*z* = 671 [CuL^4]$^+$. FT IR: ν(CO) = 1634 cm^{-1}. $C_{34}H_{28}ClCuFeN_6O_6\cdot 2H_2O$ (807.516): calcd. C 50.57, H 3.99, N 10.41; found C 50.28, H 3.62, N 10.55.

[Ni(L^1)$_2$](ClO$_4$)$_2$: UV/Vis (MLCT band; CH_3CN): λ_{max} (ε, M^{-1} cm^{-1}) = 458 nm (670). FAB$^+$ MS: *m*/*z* = 953 [Ni(L^1)$_2$](ClO$_4$)$^+$. FT IR: ν(CO) = 1603, 1645, 1714 cm^{-1}. $C_{44}H_{36}Cl_2Fe_2N_4NiO_{12}\cdot 2H_2O$ (1090.128): calcd. C 48.48, H 3.70, N 5.14; found C 47.93, H 3.63, N 5.17.

[NiL^2](ClO$_4$)$_2$: UV/Vis (MLCT band; CH_3CN): λ_{max} (ε, M^{-1} cm^{-1}) = 460 nm (140). FAB$^+$ MS: *m*/*z* = 767 [NiL^2](ClO$_4$)$^+$. FT IR: ν(CO) = 1603, 1631, 1668 cm^{-1}. $C_{34}H_{26}Cl_2FeN_4NiO_{12}\cdot 3H_2O$ (922.105): calcd. C 44.29, H 3.50, N 6.08; found C 44.49, H 3.05, N 6.20.

[Ni(L^3)$_2$](ClO$_4$)$_2$: UV/Vis (MLCT band; CH_3CN): λ_{max} (ε, M^{-1} cm^{-1}) = 445 nm (500). FAB$^+$ MS: *m*/*z* = 951 [Ni(L^3)$_2$](ClO$_4$)$^+$. FT IR: ν(CO) = 1601 cm^{-1}. $C_{44}H_{38}Cl_2Fe_2N_6NiO_{10}\cdot 2H_2O$ (1088.158): calcd. C 48.57, H 3.89, N 7.72; found C 48.97, H 3.82, N 7.74.

[NiL^4](ClO$_4$)$_2$: UV/Vis (MLCT band; CH_3CN): λ_{max} (ε, M^{-1} cm^{-1}) = 448 nm (360). FAB$^+$ MS: *m*/*z* = 765 [NiL^4](ClO$_4$)$^+$. FT IR: ν(CO) = 1605 cm^{-1}. $C_{34}H_{28}Cl_2FeN_6NiO_{10}\cdot 3H_2O$ (920.135): calcd. C 44.38, H 3.72, N 9.13; found C 44.44, H 3.53, N 9.04.

[Fe(L^1)$_2$](ClO$_4$)$_2$: UV/Vis (MLCT band; CH_3CN): λ_{max} (ε, M^{-1} cm^{-1}) = 448 nm (1610). FAB$^+$ MS: *m*/*z* = 951 [Fe(L^1)$_2$](ClO$_4$)$^+$. FT IR: ν(CO) = 1600, 1624, 1714 cm^{-1}. ^{1}H NMR (300 MHz, CD_3CN, 10 mM, 295 K): δ = 83.0 (2 H, *H*-*o*-bipy), 67.9, 56.4, 56.4 and 49.6 (2 H each, *H*-*m*-bipy), 13.8 (2 H, *H*-*p*-bipy), 7 to 0 (22 H, *H*-Cp, CH_2-bipy and *H*-*p*-bipy), −9.4 (4 H, CH_2-bipy). $C_{44}H_{36}Cl_2Fe_3N_4O_{12}\cdot 2H_2O$ (1087.275): calcd. C 48.61, H 3.71, N 5.15; found C 48.75, H 3.61, N 5.27.

[FeL^2](ClO$_4$)$_2$: UV/Vis (MLCT band; CH_3CN): λ_{max} (ε, M^{-1} cm^{-1}) = 450 nm (1100). FAB$^+$ MS: *m*/*z* = 765 [FeL^2](ClO$_4$)$^+$. FT IR: ν(CO) = 1661 cm^{-1}. ^{1}H NMR (300 MHz, CD_3CN, 10 mM, 295 K): δ = 80.5 (2 H, *H*-*o*-bipy), 62.0, 61.4, 56.6 and 17.8 (2 H each, *H*-*m*-bipy), 7.1 (2 H, *H*-*p*-bipy), 6.4 and 0.8 (4 H resp., *H*-Cp), −1.9 (2 H, *H*-*p*-bipy), −8.7 (4 H, CH_2-bipy). $C_{34}H_{26}Cl_2Fe_2N_4O_{12}\cdot H_2O$ (883.221): calcd. C 46.24, H 3.20, N 6.34; found C 45.97, H 3.10, N 6.37.

[HgL^2](CF$_3$SO$_3$)$_2$: UV/Vis (MLCT band; CH_3CN): λ_{max} (ε, M^{-1} cm^{-1}) = 432 nm (1720). FAB$^+$ MS: *m*/*z* = 961 [HgL^2](CF$_3$SO$_3$)$^+$. FT IR: ν(CO) = 1712 cm^{-1}. $C_{36}H_{26}F_6FeHgN_4O_{10}S_2$ (1109.177): calcd. C 38.98, H 2.36, N 5.05; found C 38.04, H 2.43, N 4.96.

[HgL^4](CF$_3$SO$_3$)$_2$: UV/Vis (MLCT band; CH_3CN): λ_{max} (ε, M^{-1} cm^{-1}) = 446 nm (450). FAB$^+$ MS: *m*/*z* = 959 [HgL^4](CF$_3$SO$_3$)$^+$. FT IR: ν(CO) = 1596, 1627 cm^{-1}. $C_{36}H_{28}F_6FeHgN_6O_8S_2\cdot 2H_2O$ (1143.238): calcd. C 37.82, H 2.82, N 7.35; found C 37.85, H 2.59, N 7.14.

Reagents, Instrumentation and Procedure: Acetonitrile (Rathburn, HPLC grade) was used as received. Dichloromethane was dried with neutral alumina (activity I) for at least 6 d before use. Tetra-*n*-butylammonium perchlorate (TBAP) was purchased from Fluka and dried under vacuum for 3 d at 80 °C. Electrochemical experiments were conducted in a conventional three-electrode cell under argon at 20 °C. The reference electrode was Ag/AgNO$_3$ (10 mM in CH_3CN containing 0.1 M TBAP). FAB (positive mode) mass spectra were recorded with an AEI Kratos MS 50 spectrometer fitted with an Ion Tech Ltd gun and using *m*-nitrobenzyl alcohol as matrix. ES-MS measurements were performed on a triple quadrupole mass spectrometer Quattro II (Micromass, Altrincham, UK). The ES source was heated to 80 °C. The sampling cone voltage (Vc) was 20 V to avoid any fragmentation processes. Sample solutions were introduced into the mass spectrometer source with a syringe pump (Harvard type 55 1111: Harvard Apparatus Inc., South Natick, MA, USA) with a flow rate of 4 μL min^{-1}. Calibration was performed using protonated horse myoglobin. Scanning was performed in the MCA (Multi Channel Analyser) mode, and several scans were summed to obtain the final spectrum. Elemental analyses were performed by the Service Central d'Analyses, CNRS, Lyon.

X-ray Structures: Crystals of the complexes between L^2 and M^{II} (where M^{II} is Cu^{II} or Ni^{II}) named {Cu^{II}L^2} and {Ni^{II}L^2}, respectively, were used for data collection with a STOE-IPDS diffractometer using Mo-K_α graphite-monochromated radiation (λ = 0.71073 Å). Intensity data were corrected for Lorentz and polarisation effects but not for absorption. Structure solution and refinement were performed with the SHELXTL package. A summary of the crystallographic data and structure refinement is given in Table 3. The two compounds {Cu^{II}L^2} and {Ni^{II}L^2} are isostructural. They crystallize in the *C*2/*c* space group with close cell parameters. Only the crystallization solvents are different. The crystallographically independent chemical formulae are [CuL^2]$_{1.5}$(ClO$_4$)$_3$ 0.5[(C_2H_5)$_2$O] 2.5(CH_3CN) and [NiL^2]$_{1.5}$(ClO$_4$)$_3$ [(C_2H_5)$_2$O] 1.5(CH_3CN) with a multiplicity of *Z* = 8; so there are 12 [ML^2]$^{2+}$ entities in the unit cell. All non-hydrogen atoms were refined with anisotropic thermal parameters, except for atoms of disordered solvents. Hydrogen atoms were generated in idealised positions (except for disordered solvents), riding on the carrier atoms with isotropic thermal parameters. CCDC-174044 {Cu^{II}L^2} and -174045 {Ni^{II}L^2} contain the supplementary crystallographic data for this paper. These data can be obtained free of charge at www.ccdc.cam.ac.uk/conts/retrieving.html or from the Cambridge Crystallographic Data Centre, 12, Union Road, Cambridge CB2 1EZ, UK [Fax: (internat.) + 44-1223/336-033; E-mail: deposit@ccdc.cam.ac.uk].

Acknowledgments

We warmly thank Drs. Hélène Nierengarten and Alain van Dorrselaer from the Laboratoire de Spectrométrie de Masse Bioorganique, at the ECPM in Strasbourg for their expertise in the ES-MS measurements.

[1] M. Buda, J.-C. Moutet, E. Saint-Aman, A. De Cian, J. Fischer, R. Ziessel, *Inorg. Chem.* **1998**, *37*, 4146.
[2] A. Ion, J.-C. Moutet, E. Saint-Aman, G. Royal, S. Tingry, J. Pecaut, S. Menage, R. Ziessel, *Inorg. Chem.* **2001**, *40*, 3632.
[3] M. Buda, J.-C. Moutet, A. Pailleret, E. Saint-Aman, R. Ziessel, *J. Electroanal. Chem.* **2000**, *484*, 164.
[4] M. Buda, A. Ion, J.-C. Moutet, E. Saint-Aman, R. Ziessel, *J. Electroanal. Chem.* **1999**, *469*, 132.
[5] J. C. Medina, T. T. Goodnow, M. T. Rojas, J. L. Atwood, A. E. Kaifer, G. K. Gokel, *J. Am. Chem. Soc.* **1992**, *114*, 10583.
[6] S. R. Miller, D. A. Gutowski, Z. H. Chen, G. K. Gokel, L. Echegoyen, A. E. Kaifer, *Anal. Chem.* **1988**, *60*, 2021.
[7] I. Ion, J.-C. Moutet, A. Popescu, L. Tomazeswki, I. Gauthier-Luneau, *J. Electroanal. Chem.* **1997**, *440*, 145.
[8] H. Scholl, K. Sochaj, *Electrochim. Acta* **1991**, *36*, 689.
[9] C. Dietrich-Bucheker, J.-P. Sauvage, J.-M. Kern, *J. Am. Chem. Soc.* **1989**, *111*, 7791 and refs. therein.
[10] B. J. Henne, D. E. Bartak, *Inorg. Chem.* **1994**, *23*, 369.
[11] M.-N. Collomb, A. Deronzier, C. Duboc Toia, M. Fontecave, K. Gorgy, J.-C. Leprêtre, S. Ménage, *J. Electroanal. Chem.* **1999**, *469*, 53.
[12] R. Ziessel, J.-M. Lehn, *Helv. Chim. Acta* **1990**, *73*, 1149.

Receiced November 21, 2001
[I01468]